ISSN (Print) : 0974-6846
Indian Journal of Science and Technology, *Vol 10(17), DOI: 10.17485/ijst/2017/v10i17/111402, April 2017* ISSN (Online) : 0974-5645

Modelling of a High Power Microwave (HPM) Source using 300 KV Marx Generator and Horn Type Antenna

Sharmila Petkar[1], Sachin B. Umbarkar[1], Faruk Kazi[2] and Navdeep M. Singh[2]

[1]Department of Electrical Engineering, Ramrao Adik Institute of Technology, Navi Mumbai – 400706, Maharashtra, India; profsjpetkar@gmail.com, sachin.umb@gmail.com
[2]Department of Electrical Engineering, Veermata Jijabai Technological Institute, Mumbai – 400031, Maharashtra, India; fskazi@vjti.org.in, nmsingh@vjti.org.in

Abstract

Objectives: To analyse a High Power Microwave (HPM) source connected to a horn antenna by a mathematical model and feeding it with various pulse shapes to find its response. To estimate the E far-field produced and compare it with experimental measurements. **Methods/Statistical analysis:** A HPM source is built using spark gap switch and Marx generator. Efforts are made to reduce the rise time of the radiated pulse by experimentally varying the spark gap distance and using different gases as di-electric medium. A peaking switch was then designed that could achieve a rise time of 1 nS. The energy discharged at the spark gap (peaking switch) is radiated using a horn type antenna. **Findings:** In the numerous simulations it was found that a sharp rising edge of the radiated pulse can be achieved if we could minimize the peaking stage inductance. A sharp rising edge gives high peak radiated power resulting in higher E far-field intensity, which is useful for the intended applications of HPM systems. Experimental results to measure the E far-field were coherent with the mathematical model; however, in order to make the mathematical model more accurate with the practical results, a scaling factor was empirically derived. **Application/Improvements:** During the experiments a range field product ($r.E_{far\text{-}field}$) of more than 200 kV was achieved. Although this compares well with some of the contemporary systems. It is much less than 7.2 MV reported elsewhere. To achieve it, some improvements are required to further reduce the rise time of radiated pulse. This can be done by better impedance matching of the radiating antenna with the peaking stage and improvement in the Marx generator switching stages .

Keywords: HPM, Pulser, PFN (Pulse Forming Network), Spark-Gap

1. Introduction

High energy impulse systems are required for electronic equipment testing against electromagnetic pulse effect. They also find application in ground penetrating radar and Electronic Warfare (EW) systems[1,2]. The high radiation power systems are built using capacitor banks that produce a sharp discharge resulting in wide band of radiated power. A faster rise time of the discharge pulse, results in wider band and higher energy density of the radiated power. In this paper, we are modelling a Marx generator employing 20 stages of capacitor banks producing 300 kV at the discharge gap. The Marx generator is connected to a peaking switch operating under pressurized SF_6 gas. The peaking switch has been designed to give a fast (1ns rise time) impulse. Further,

* *Author for correspondence*

the impulse is radiated using a horn-type antenna to convert this compact High Voltage (HV) system into an UWB system[3,4]. A Mark generator end section is attached to peaking stage as indicated in Figure 1. Marx generator circuit and the peaking stage were operated at the same gas (SF6) pressure[5]. The capacitor bank could not sustain higher electric field intensity raised in proportion to the rise of gas pressure more than 0.5 kg/cm^2 (0.48 bar). This limitation was overcome by redesigning the arrangement of peaking stage. To conduct the experiment at higher pressure on peaking stage, further development of the peaking switch was carried out. This development isolates the peaking stage from the Marx circuit. The peaking switch now has 55 mm thick wall of derlin material, which can withstand up to 13.5 Kg/cm^2 (13.2 bar)gas pressure. However, it was found that gas pressure of 2 kg/cm^2 at the peaking switch is sufficient to generate the desired electric field[4]. The diameter of the electrode is 37 mm and the gap distance between electrodes can be varied from 0.5 mm to 10mm.Variation in the inter electrode gap distance changes inductance of the peaking switch. The peaking switch is as shown in Figure 2. The objective of this study is to analyze a compact, fast transient, HV radiating system for generating a high intensity electromagnetic field.

1.1 Radiating Stage Simulink Model

The pulse power system in mainly operates on capacitor discharging phenomenon. The model for Marx Generator as RLC circuit is designed in MALAB environment. The peaking stage and load are connected to the E far field. Model for the verification in MATLAB is shown in Figure 3. Interlinking capacitor bank between each stage have a value of 7200pF (6 x 1200 pF capacitors). The equivalent capacitance of the 20 stages Marx circuit (C1) having a capacitance of 7200 pF at each stage is 360 pF. The capacitance of the final (peaking) stage (C2) is 62.5 pF and the spark gap of the peaking switch has a capacitance of 48 pF (C3), which is in parallel with resistance-inductance (R1-L1) of the spark-gap[6,7]. This model is excited with various shapes of input feeding pulse. In[8] observed that the radiated E far field intensity increases as the rise time of the discharge pulse decreases. It was found after numerous simulations that the nature of the radiated

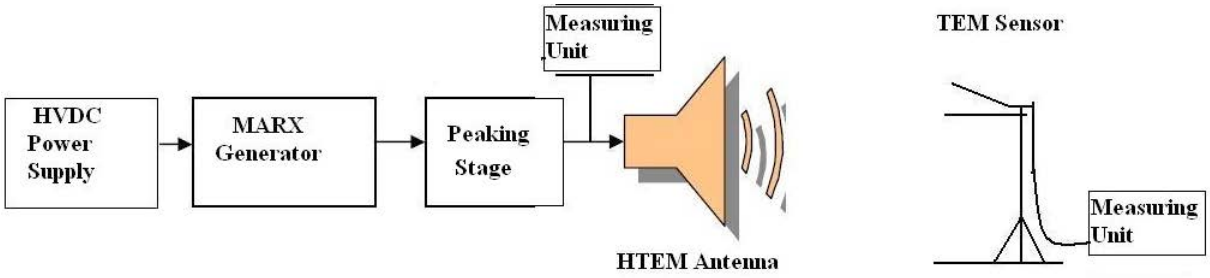

Figure 1. Block diagram of electromagnetic field generator.

(a) Switch outer view (b) Inner side HV Electrode (c) Inner side LV Electrode

Figure 2. Peaking switch.

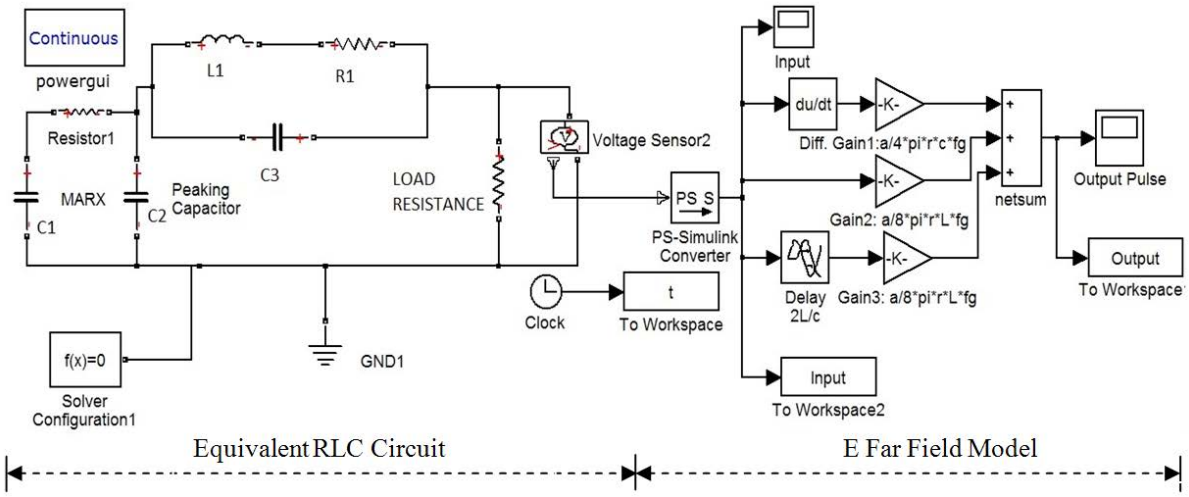

Figure 3. The RLC modelling for the far field radiation.

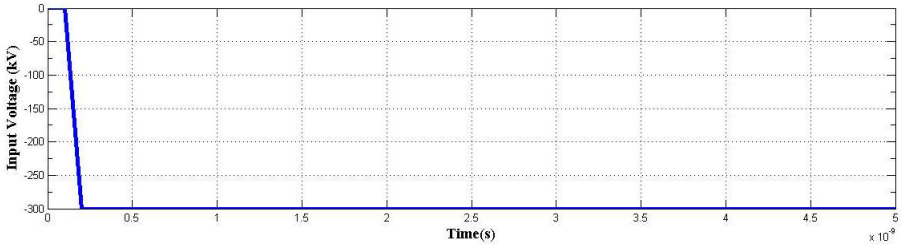

Figure 4(a). Inverted step input pulse.

E far field intensity exhibits inverted derivative plot of the input feeding pulse shown in Figure 4 and Figure 5.

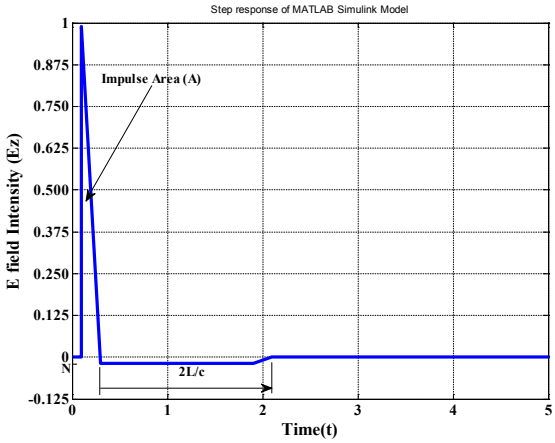

Figure 4(b). Radiated output pulse for step input pulse.

Results of the mathematical model in Simulink are shown in Figure 3, show good co-relation with experimental work. The calculation for characteristic impedance of the peaking stage (the last stage capacitor) together with peaking switch in Laplace domain is given in equation (1) to (7).

$$\frac{1}{C_T} = \frac{1}{C_2} + \frac{1}{C_3} \quad (1)$$

$C_T = 27.1$ pF

$C_T(s) = 2.71 \times 10^{10}$ (2)

The resultant impedance (Z1) for the spark gap is given in equation (3).

$$Z_1 = \frac{(10^5 s + 0.5\times10^5)}{(s^2 + 0.5s + 5\times10^6)} \quad (3)$$

$$V_1(s) = V_2(s) + Z_1.a \quad (4)$$

Where,

$$a = \frac{V_2(s)}{180} \quad (5)$$

Put equation (3) and (5) in equation (4) gives equation (6).

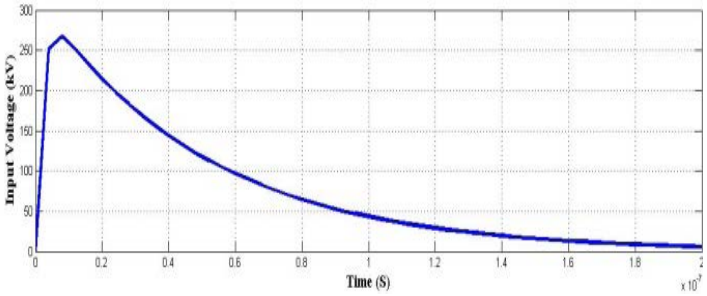

Figure 5(a). Exponential decaying input pulse.

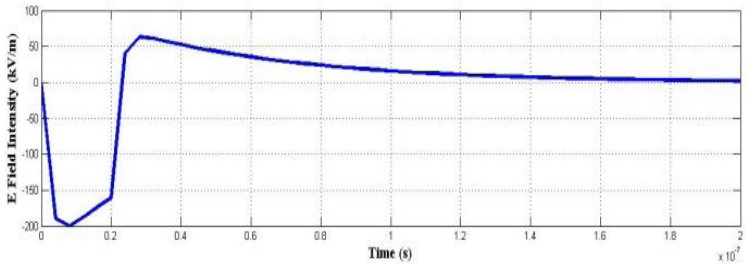

Figure 5(b). Radiated output pulse for exponential decaying input pulse.

$$V_1(s) = V_2(s) + \frac{(10^5 s + .5\times10^5)}{(s^2 + 0.5s + 5\times10^6)}\left(\frac{V_2(s)}{180}\right) \quad (6)$$

The response of model is given in equation (7).

$$V_2(t) = 300\times10^3 - (751.397)\left[e^{278.05t}\sin(2.218\times10^5\right]t \quad (7)$$

The step response of the Simulink model is given in Figure 4(b). The exponential decay response is given in Figure 5(b).

2. Mathematical Modeling of the Radiated Field

In impulse radiating type of antenna, the radiation starts at the rising instant of the pulse[9]. When the pulse is detached from the antenna, it has either spherical wave or uniform plane wave pattern. If the antenna is reflective type, then the radiated pulse is uniform-plane-wave and if the antenna is HTEM type, then the radiated pulse is spherical[3]. The equation (15) gives the total 'E' far field intensity[10,11]. Figure 6 shows the side and top view of the TEM horn antenna with its geometrical parameters, where 'L' is the length, 'w' is the width, 'a' is the aperture height, 'Θa' is the tapering angle, and 'α' is the flair angle of the antenna.

Equation (8) to (11) gives optimal geometrical relationships[11,12]

$$w = 2L\tan(\alpha/2) \quad (8)$$

$$a = L\sin\theta_a \quad (9)$$

$$\frac{w}{a} = \frac{2\tan(\alpha/2)}{\sin\theta_a} \quad (10)$$

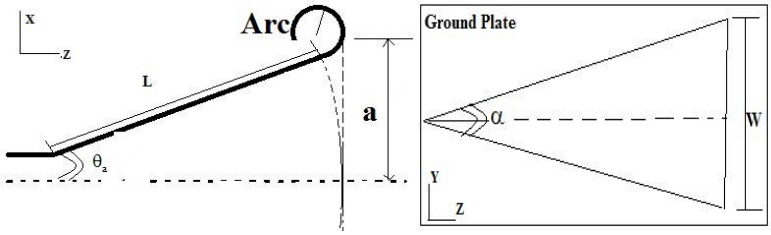

Figure 6. Side view and top view of antenna.

$$\alpha = 2\arctan\left[\frac{w}{2a}\sin(\theta_a)\right] \quad (11)$$

The characteristic impedance of the Impulse Radiating Antenna (IRA) plays an important role in the radiated field intensity. This parameter is based on the geometrical structure of the antenna. The shape of the HTEM antenna is not parallel to ground plate. Thus it is an important task to calculate the characteristic impedance at high frequency non parallel structure[6].

Equation (12) and (13) gives the characteristic impedance[5] (Zc) for $w/a > 1$ and $w/a < 1$.

$$Z_c = 2\times\frac{377}{(w/a)+2} \quad (12)$$

$$Z_c = 2\times 138\times\log\frac{8}{(w/a)} \quad (13)$$

The width 'w' of the horn and height 'a' have to be chosen such that the characteristic impedance Zc should be 377 Ohm to match with the characteristic impedance of free space.

'Zc' and the intrinsic impedance 'Zo' is used to find the geometric impedance (fg), given by equation (14).

$$f_g = \frac{Z_c}{Z_0} \quad (14)$$

The total radiated E field in the forward axis is given in equation (15).

$$E(r,t) = -\frac{V_o}{r}\frac{a\wp}{4\pi c f_g}\left[\delta(t) - \frac{c}{2L}[u(t) - u(t-\frac{2L}{c})]\right] \quad (15)$$

Where, r is the forward axis distance. Expressing the above equation in terms of theta (θ) (tapering angle) of the antenna, gives equation (16).

$$E(r,\theta_a,t) = -\frac{V_o}{r}\frac{a\wp}{4\pi c f_g}\left[\delta(t) - \frac{c\sin\theta_a}{2a}\left[u(t) - u\left(t - \frac{2}{c}\left(\frac{a}{\sin\theta_a}\right)\right)\right]\right] \quad (16)$$

Where, $\delta(t)$ is the delta function?

The total radiated field depends on Θa, r, fg and dV/dt is shown in equation (16) and is modified to (18) by using (17)[12].

$$\theta_a = \sin^{-1}\left[2\left(\frac{a}{w}\right)\tan\left(\frac{\alpha}{2}\right)\right] \quad (17)$$

$$E(r,\alpha,t) = -\frac{V_o}{r}\frac{a\wp}{4\pi c f_g}\left[\delta(t) - \frac{c}{w}\tan(\alpha/2)\left[u(t) - u\left(t - \frac{w}{c}\frac{1}{\tan(\alpha/2)}\right)\right]\right] \quad (18)$$

Orientation of antenna has tapered length along z-axis and flared along y- axis.

In equation (18), r=15 m, a=0.4 m, L=1.2 m, fg=0.1733, $\wp$=1 is the unit less scaling factor. So E far field calculated from equation (15) is 25.01kV/m. This calculation differs from experimental reading. Thus, it is required to modify the scaling factor ($\wp$) so that the E far field calculation matches to the experimental values. The experiments are conducted in free space using TEM sensor probes. Thus, the suggested scaling factor to improve the accuracy of the analytical calculation is given in (19).

$$\wp = 90\left(\frac{a}{L}\right)^2 \text{ Unit-less.} \quad (19)$$

Thus the approximated simplified analytical equation (18) is represented in terms of exact solution which match with the experimental value is given in (20).

$$E(r,\alpha,t) = -\frac{V_o}{r}\frac{45a^3}{2\pi c f_g L^2}\left[\delta(t) - \frac{c}{w}\tan(\alpha/2)\left[u(t) - u\left(t - \frac{w}{c}\frac{1}{\tan(\alpha/2)}\right)\right]\right] \quad (20)$$

The next section elaborates experimental validation.

3. Experimental Validation

The experiments were carried out in free space at different SF6 gas pressures inside Marx generator and switch. The experimental setup is shown in Figure 7.

Figure 7. Experimental setup.

The radiated fields are measured up to 24 meter using TEM sensor probes. The measured values are given in Table 1. The effective aperture height of TEM sensor is 12.5 mm. The 5 degree deviation from the bore-sight of antenna resulted in drop of E far field intensity from 20 kV/m at 10m distance from the antenna to 0.8 kV/m. This indicates high directivity of the antenna. The maximum 'E far field' of the antenna is achieved at 0.5 kg/cm2 pressure of SF6 gas inside the Marx generator and 2 kg/cm2 SF6 gas pressure inside peaking switch. At 15m distance from the antenna along its bore sight axis, E far amplitude is measured which is found to be 14.4 kV/m, as reported in Figure 8. The measurement and relevant calculations are explained below as given by equations (21) and (22).

$$V_{osc}(t) = h_{eff}.E_{inc}(t).\frac{R_{load}}{R_{load}+R_{antenna}} \quad (21)$$

The probe having characteristics impedance of 50 ohm is required to be maintained. Thus w and a, is varied throughout the geometry of TEM sensor. To get constant 50 ohm impedance width(w) is 327mm and aperture height (a) is 25 mm, the effective height of aperture for half TM sensor is a/2=12.5 mm.TEM sensor[13] has Rload=Rantenna=50Ω; heff = 12.5mm is the effective height, Einc(t) is the incident E far field intensity[14]. Thus, the above equation can be reduced to equation (22).

$$E_{inc}(t) = \frac{2V_{osc}(t)}{12.5} kV/m \quad (22)$$

- Oscilloscope reading: 3.6 div × 1 V/div × 25x = 90 Volts

Table 1 indicates the experimental results which are carried out for various SF6 gas pressure. Sensors are moved from 15m to 24 m and 0 deg to ±5 deg.

Mathematical calculated values of E are compared with the measured value of radiated E far field intensity as per equation (20). It shows good agreement with each other.

4. Wavelet Transform

The waveform recorded using oscilloscope is non stationary that has higher frequency components, which can be analysed using wavelet transformation[15]. The wavelet transform is a modern technique that finds application in the analysis of wave propagation, signal processing, image processing and physics. We use wavelet transform here for the analysis of the transient E far afield as it allows components of complex and non-stationary signals analysis. A wavelet means a small oscillating

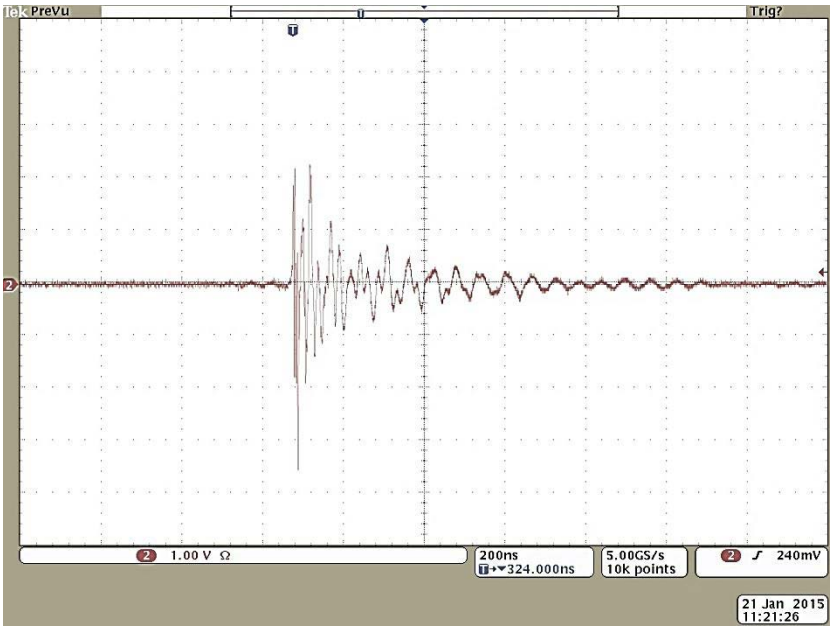

Figure 8. The E far field amplitude is 14.4 kV/m

Table 1. Experimental results

Position of Sensor from Focal Point	SF6 gas Pressure in Marx / Peaking Switch (Kg/cm2)	E far field (kV/m)	r.Efar_ field (kV)	Charging Voltage Vmax (kV)	VPeak Feeding pulse (kV)	"Gain factor" $\frac{r.E_{far_{Field}}}{Vpeak}$
15m, 0o	Air/air	7.6	114	12	120	0.95
15m, 0o	0.2/1	8.6	129	16	160	0.81
15m, 0o	0.2/2	9.0	135	14	140	0.96
15m, 0o	0.2/3	8.8	132	16	160	0.83
15m, 0o	0.2/4	10.2	153	16	160	0.96
15m, 0o	0.2/5	10.2	153	16	160	0.96
15m, 0o	0.2/6	10.4	156	16	160	0.97
15m, 0o	0.2/7	10.4	156	16	160	0.97
15m, 0o	0.2/8	10.4	156	16	160	0.97
15m, 0o	0.3/1	13	195	20	200	0.975
15m, 0o	0.3/2	13	195	20	200	0.975
15m, 0o	0.3/3	12.8	192	20	200	0.96
15m, 0o	0.3/4	12.6	189	19	190	0.99
15m, 0o	0.3/5	12.8	192	20	200	0.96
15m, 0o	0.3/6	12.4	186	19	190	0.98
15m, 0o	0.3/7	12.4	186	19	190	0.98
15m, 0o	0.3/8	12.2	183	19	190	0.96
15m, 0o	0.5/1	13.4	201	24	240	0.84
10m, 0o	0.5/2	20	200	24	240	0.833
15m, 0o	0.5/2	14.4	216	24	240	0.9
20m, 0o	0.5/2	10.4	208	24	240	0.867
24m, 0o	0.5/2	6.4	153.6	22	220	0.698
15m,5o (Left-Side)	0.5/2	0.8	12	22	220	0.05
15m, 5o (Right-Side)	0.5/2	0.8	12	22	220	0.05

wave whose amplitude begins at zero, increases, and then decays quickly back to zero in time domain. Wavelet transform provides the time-frequency representation of the signal i.e. it gives the frequency of the signals and the time associated to those frequencies. This is the advantage of Wavelet transform over Fourier transform, which gives the spectral content of the signal, but doesn't give any information regarding the time those spectral components appear. The Continuous Wavelet Transforms (CWT) of time domain signal x (t) is defined by equation (23).

$$CWT(b,a) = \frac{1}{\sqrt{a}} \int_{-\infty}^{\infty} x(t) \psi^* \left(\frac{t-b}{a} \right) dt \qquad (23)$$

Where, 'a' is the scale parameter, 'b' is the translation (time) parameter, $\Psi(t)$is the analysing function; also called mother wavelet, $\psi^*\left(\frac{t-b}{a}\right)$

is the scaled and time translated complex conjugation wavelet function. Figure 9(a) shows the time-amplitude representation of the given test signal of 4.9 kV. Figure 9(b) represents the Frequency spectrum (Fourier Transform) of the radiated field. Dominant frequency of the signal is near about 35MHz. Figure 10 shows the wavelet transforms of the radiated field which is capable of providing time and frequency information simultaneously[15,10]. The peak in the Figure 13 corresponds to the frequency of the signal. Here, the Morlet wavelet is used as mother wavelet.

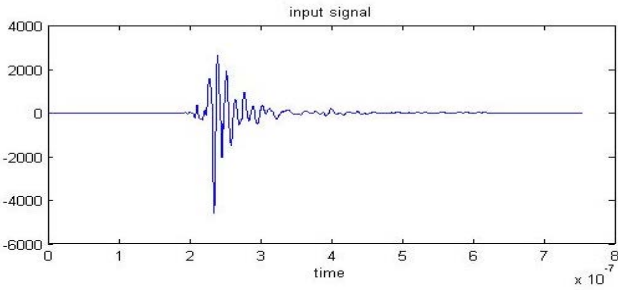

Figure 9(a). Time-amplitude representation of the radiated E far field - 4.9 kV/m.

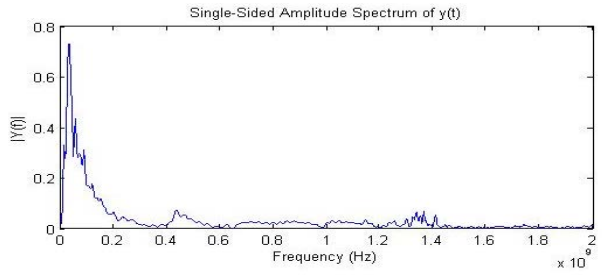

Figure 9(b). Frequency spectrum of radiated E far field.

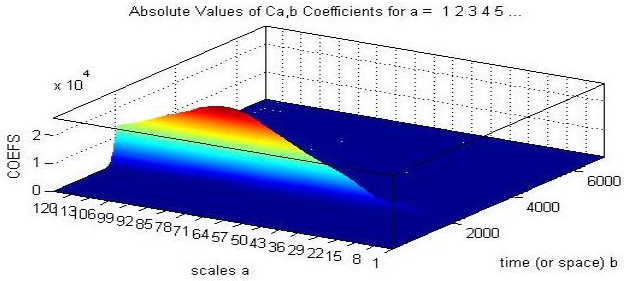

Figure 10. Wavelet spectrum.

5. Conclusion

Analysis of a High Power Microwave (HPM) source that uses a Marx generator is attempted. The system can work as an ultra-wideband source of radiated power. This was achieved by designing the last stage of the Marx circuit to be connected to a spark gap (peaking switch). The radiated power from the spark gap switch is directed into the free space using a horn type antenna. The RLC model of the system is operated at various shapes of feed pulse and it is observed that the radiated pulse is the inverted derivative of the input feeding pulse. The peaking stage plays an important role in pulse sharpening and its inductance should be kept at a minimum to get the low rise time pulse. MATLAB-SIMULINK model shows The working principle of pulse forming network (Marx generator) and the peaking switch to form a low rise time (1ns) pulse is shown with the help of MATLAB-SIMULINK model while the CST Microwave Studio modelling shows the radiation process of generated pulse by antenna and its spectrum analysis is carried out by wavelet transform. The mathematical model for E far field is modified by introducing a new empirical scaling factor ($\wp$) that gives results, which are validated with the experimental values.

6. Acknowledgement

The authors would like to thank Dr. Vijay D patil (President, DY Patil Group Navi-Mumbai), Dr. Ramesh Vasappanavara (Principal, RAIT), Prof. O G Kakde (Director-VJTI) for their continuous support and encouragement.

7. References

1. Giri DV. High-power electromagnetic radiators: Nonlethal weapons and other applications. Harvard University Press; 2004.
2. Verma R, Shyam A, Chaturvedi S, Kumar R, Lathi B, Sarkar P, Chaudhari V, Shukla R, Debnath K, Sharma S, Sonara J, Shah K, Adhikary B, Jigna T, Piyush J. Impulse electromagnetic interference generator. In the 26th International Conference on Power Modulator Symposium and High voltage Workshop; 2004 May. p. 543–6.
3. Baum CE. JOLT: A highly directive, very intensive, impulse-like radiator. Sensor and Simulation Notes. 2003 Nov; 480:1–36.
4. Bindu S, Magalvedekar HA. Electro-dynamic simulation of high-voltage peaking switch. Institute of Electrical and Electronics Engineers (IEEE) Transaction on Plasma Science. 2012 Nov; 40(11):3093–9. Crossref.
5. Tewari SV, Umbarkar SB, Agarwal R, Saroj PC, Sharma A, Mittal KC et al. Development and analysis of PFN based Marx generator finite integration technique for an antenna load. Institute of Electrical and Electronics Engineers (IEEE) Transaction on Plasma Science. 2013 Oct; 41(10):2684–90. Crossref.
6. Umbarkar SB, Bindu S, Mangalvedekar HA, Sharma A, Saroj PC, Mittal KC. Analysis of half TEM horn antenna for high power UWB system. In the 19th Institute of Electrical and Electronics Engineers (IEEE) Conference on Pulsed Power; 2013 Jun. p. 1–6.
7. Umbarkar SB, Bindu S, Mangalvedeker HA, Sharma A, Chakravarthy DP, Saroj PC, Mittal KC, Chakravarthy DP. Modeling and analysis of half TEM horn antenna and jolt antenna for high power UWB application: a comparative

study. The National Symposium on High Power RF & Microwaves (HPRFM), Gujarat, India; 2013 Sep 4–6.
8. Andrews JR. UWB signal sources, antennas and propagation. Picosecond Pulse Labs; 2003 Aug. p. 1–11.
9. Baum CE, Farr EG, Giri DV. Review of impulse-radiating antennas. Stone WR editor, Oxford University Press. 1999; 16:403–39.
10. Farr EG, Baum CE. A model of small-angle TEM horns. Sensor and Simulation Notes; 1992. p. 340.
11. Kolokotronis DA, Huang Y, Zhang JT. Design of TEM horn antennas for impulse radar. High Frequency Postgraduate Student Colloquim, University of Leeds. 1999 Sep; 2(2):1–9.
12. Abramowitz M, Stegun IA. Handbook of mathematical function. National Bureau of standards; 1967. p. 1–1040.
13. Ludeking L, Woods A, Cavey L. Magic user manual 3.2. Alliant Techsystems, U.S.A; 2011.
14. Lehr JM, Burger JW, Prather WD, Hull J, Abdalla MD, Skipper MC, Giri DV. Evaluation of resistors for transient high-voltage applications. 12th Institute of Electrical and Electronics Engineers (IEEE) International Conference Pulse power conference, Monterey, CA; 1999 Jun. p. 666–9. Crossref
15. Sifuzzaman M, Islam MR, Ali MZ. Applications of the wavelet transform and its advantages compared to the Fourier transform. Journal of Physical Science. 2009 Oct; 13:121–34.